Electronic Supplementary Information For

Structural Characterization and Proton Reduction Electrocatalysis of Thiolate-Bridged Bimetallic (CoCo and CoFe) Complexes

Peng Tong, Wenjie Xie, Dawei Yang, Baomin Wang, Xiaoxiao Ji, Jianzhe Li and Jingping Qu *

State Key Laboratory of Fine Chemicals, School of Pharmaceutical Science and Technology, Faculty of Chemical, Environmental and Biological Science and Technology, Dalian University of Technology, 2 Linggong Road, Dalian 116024, P. R. China

Contents

Table S1 Crystallographic data for **1[PF_6]**·CH_2Cl_2, **2**

	1[PF_6]·CH_2Cl_2	**2**
Formula	$C_{27}H_{36}Cl_2Co_2F_6IPS_2$	$C_{26}H_{34}Co_2S_2$
Formula weight	885.31	528.51
Crystal dimensions (mm^3)	0.34 × 0.32 × 0.28	0.33 × 0.32 × 0.31
Crystal system	Monoclinic	Triclinic
Space group	P21/c	P−1
a (Å)	8.6584(9)	9.4287(4)
b (Å)	14.3968(15)	9.5832(4)
c (Å)	27.102(3)	15.4379(9)
α (°)	90.00	103.950(2)
β (°)	93.701(2)	100.074(2)
γ (°)	90.00	108.7400(10)
Volume ($Å^3$)	3371.3(6)	1232.73(10)
Z	4	2
T (K)	220(2)	293(2)
D_{calcd} (g cm^{-3})	1.744	1.424
μ (mm^{-1})	2.281	1.526
F (000)	1760	552
No. of rflns. collected	29822	11882
No. of indep. rflns. /R_{int}	5819 / 0.0376	4345 / 0.0344
No. of obsd. rflns. [$I_0 > 2\sigma(I_0)$]	5036	3855
Data / restraints / parameters	5819 / 467 / 435	4345 / 0 / 271
R_1 / wR_2 [$I_0 > 2\sigma(I_0)$][a]	0.0772 / 0.1637	0.0338 / 0.1172
R_1 / wR_2 (all data)[a]	0.0893 / 0.1699	0.0402 / 0.1272
GOF (on F^2)[a]	1.014	1.057
Largest diff. peak and hole (e $Å^{-3}$)	1.194 / −1.170	0.436 / −0.637

Table S2 Crystallographic data for **3[PF_6]**, **3** and **4[BF_4]**

	3[PF_6]	**3**	**4[BF_4]**
Formula	$C_{25}H_{31}CoF_6FePS_2$	$C_{25}H_{32}CoFeS_2$	$C_{26}H_{35}BCo_2F_4S_2$
Formula weight	655.37	511.41	616.33
Crystal dimensions (mm^3)	0.33 × 0.31 × 0.24	0.32 × 0.31 × 0.24	0.35 × 0.32 × 0.28
Crystal system	Monoclinic	Triclinic	Monoclinic
Space group	C2/m	P−1	P2(1)/c
a (Å)	16.773(5)	10.5974(10)	9.7866(10)
b (Å)	15.626(5)	11.0324(11)	12.0453(12)
c (Å)	10.675(3)	12.0904(12)	23.210(2)
α (°)	90.00	79.404(2)	90.00
β (°)	103.051(4)	66.981(2)	95.489(2)
γ (°)	90.00	67.518(2)	90.00
Volume ($Å^3$)	2725.4(15)	1201.1(2)	2723.5(5)
Z	4	2	4
T (K)	296(2)	100(2)	293(2)
D_{calcd} (g cm^{-3})	1.597	1.414	1.503
μ (mm^{-1})	1.407	1.477	1.412
F (000)	1340	534	1272
No. of rflns. collected	7400	8015	31966
No. of indep. rflns. /R_{int}	2499 / 0.0215	4226 / 0.0294	4777 / 0.0424
No. of obsd. rflns. [$I_0 > 2\sigma(I_0)$]	2279	3721	4268
Data / restraints / parameters	2499 / 0 / 172	4226 / 0 / 262	4777 / 7 / 320
R_1 / wR_2 [$I_0 > 2\sigma(I_0)$][a]	0.0352 / 0.1158	0.0405 / 0.0998	0.0360 / 0.0906
R_1 / wR_2 (all data)[a]	0.0384 / 0.1186	0.0453 / 0.1026	0.0423 / 0.0944
GOF (on F^2)[a]	0.994	1.000	1.002
Largest diff. peak and hole (e $Å^{-3}$)	0.660 / −0.368	1.010 / −0.758	0.419 / −0.412

Fig. S1 ORTEP diagram of **1[PF_6]**·CH_2Cl_2

Hydrogen atoms, one CH_2Cl_2 molecule and counteranion PF_6^- are omitted for clarity (thermal ellipsoids shown at 30% probability)

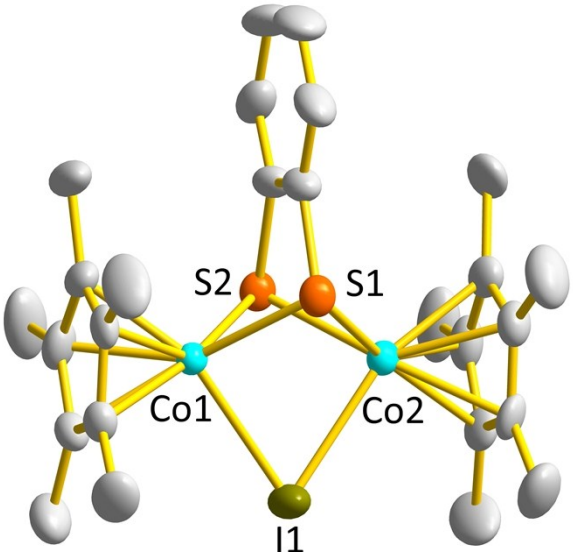

Table S3 Selected bond distances (Å) and bond angles (°) for **1[PF_6]**·CH_2Cl_2

Distances (Å)			
Co1–Co2	2.969 (2)	Co1–S1	2.276(3)
Co1–S2	2.282(2)	Co2–S1	2.278(3)
Co2–S2	2.287(2)	Co1–I1	2.587(2)
Co2–C25	2.575(2)	Co1–Cp*1	1.684(2)
Co2–Cp*2	1.691(2)		
Angles (°)			
Co1–S1–Co2	81.39(8)	Co1–S2–Co2	81.05(8)
S1–Co1–I1	86.98(7)	S2–Co1–I1	89.28(7)
Torsion angles (°)			
S1–Co1Co2–S2	113.13(12)	Co1–S1S2–Co2	114.55 (11)
Cp*1–Cp*2	1.77 (44)		

Fig. S2 ORTEP diagram of **2**

Hydrogen atoms are omitted for clarity (thermal ellipsoids shown at 30% probability)

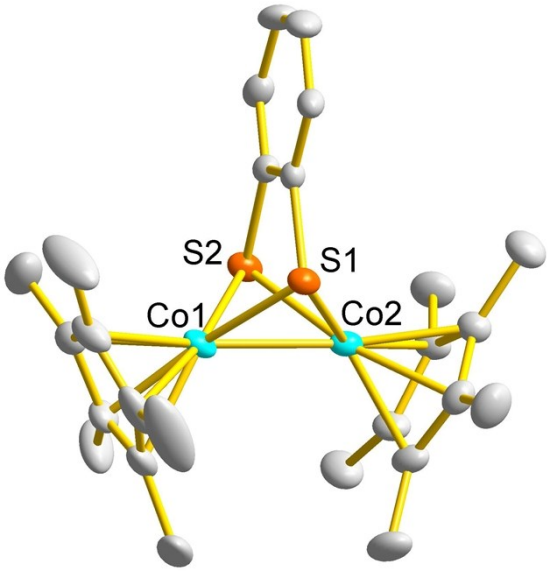

Table S4 Selected bond distances (Å) and bond angles (°) for **2**

Distances (Å)			
Co1–Co2	2.444(1)	Co1–S1	2.210(1)
Co1–S2	2.213(1)	Co2–S1	2.223(2)
Co2–S2	2.212(2)	Co1–Cp*1	1.673(1)
Co2–Cp*2	1.670(1)		
Angles (°)			
Co1–S1–Co2	66.91(2)	Co1–S2–Co2	67.06(2)
S1–Co1–Co2	56.81(2)	S2–Co1–Co2	56.47(2)
S1–Co2–Co1	56.27(3)	S2–Co2–Co1	56.48(2)
Torsion angles (°)			
S1–Co1Co2–S2	106.63(3)	Co1–S1S2–Co2	95.84(4)
Cp*1–Cp*2	53.07(13)		

Fig. S3 ORTEP diagram of **3[PF_6]**

Hydrogen atoms, except one hydrogen atom of C_5Me_4H and counteranion PF_6^- are omitted for clarity (thermal ellipsoids shown at 30% probability)

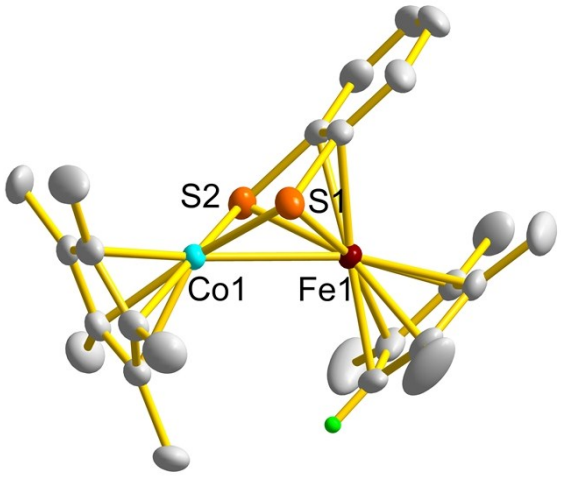

Table S5 Selected bond distances (Å) and bond angles (°) for **3[PF_6]**

Distances (Å)			
Fe1–Co1	2.796(1)	Co1–S1	2.157(2)
Fe1–S1	2.322(2)	Co1–S2	2.156(1)
Fe1–S2	2.314(1)	Fe1–Cp*1	1.652(1)
Co2–Cp*2	1.700(1)		
Angles (°)			
Fe1–S1–Co1	77.15(3)	S1–Fe1–S2	83.29(3)
S1–Co1–S2	91.15(3)	Co1–Fe1–S1	48.80(2)
Fe1–Co1–S1	54.06(2)		
Torsion angles (°)			
S1–Fe1Co1–S2	124.07(4)	Fe1–S1S2–Co1	119.02 (5)
Cp*1–Cp*2	72.26(15)		

Fig. S4 ORTEP diagram of **3**

Hydrogen atoms and one hydrogen atom of C_5Me_4H are omitted for clarity (thermal ellipsoids shown at 30% probability)

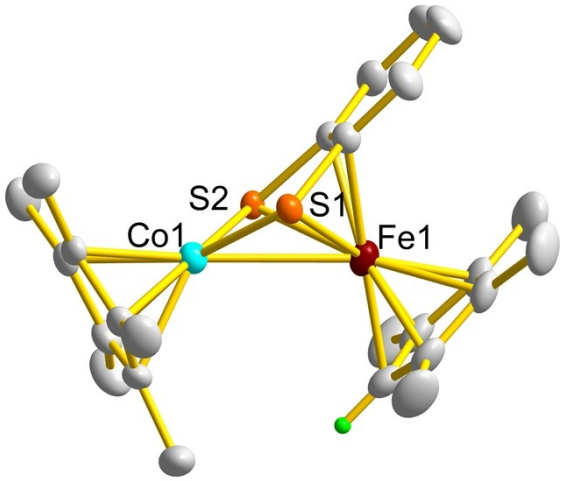

Table S6 Selected bond distances (Å) and bond angles (°) for **3**

Distances (Å)			
Fe1–Co1	2.612(2)	Co1–S1	2.134(2)
Fe1–S1	2.247(2)	Co1–S2	2.134(2)
Fe1–S2	2.247(2)	Fe1–Cp*1	1.686(1)
Co2–Cp*2	1.666(1)		
Angles (°)			
Fe1–S1–Co1	73.14(3)	S1–Fe1–S2	85.89(5)
S1–Co1–S2	91.69(5)	Co1–Fe1–S1	51.43(2)
Fe1–Co1–S1	55.42(2)		
Torsion angles (°)			
S1–Fe1Co1–S2	121.24 (5)	Fe1–S1S2–Co1	112.96(4)
Cp*1–Cp*2	70.64(13)		

Fig. S5 ORTEP diagram of **4[BF_4]**

Hydrogen atoms except for the bridging hydrogen between two Co atoms and counteranion BF_4^- are omitted for clarity (thermal ellipsoids shown at 30% probability)

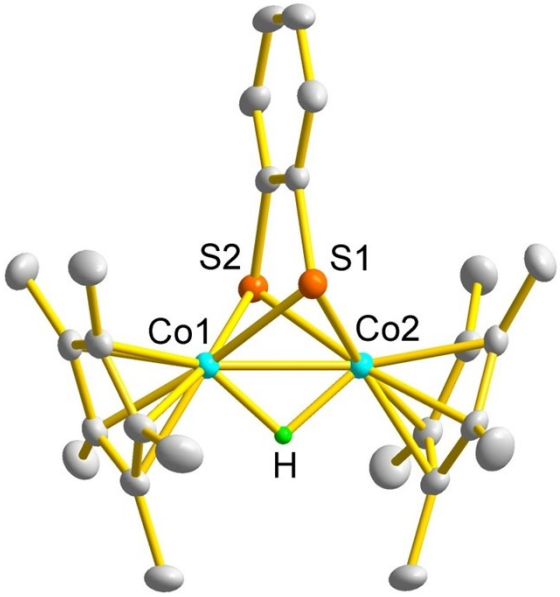

Table S7 Selected bond distances (Å) and bond angles (°) for **4[BF_4]**

Distances (Å)			
Co1–Co2	2.412(1)	Co1–S1	2.246(1)
Co1–S2	2.246(2)	Co2–S1	2.249(1)
Co2–S2	2.246(1)	Co1–H	1.57(4)
Co2–H	1.60(4)	Co1–Cp*1	1.650(1)
Co2–Cp*2	1.652(1)		
Angles (°)			
Co1–S1–Co2	64.91(2)	Co1–S2–Co2	64.95(2)
Co1–H1–Co2	98.55(178)		
Torsion angles (°)			
S1–Co1Co2–S2	102.68(4)	Co1–S1S2–Co2	91.05(4)
S1–Co1Co2–H1	128.09(181)	S2–Co1Co2–H1	129.23(181)
Cp*1–Cp*2	41.42(12)		

Fig. S6 ESI-HRMS of **1[PF_6]** in CH_2Cl_2

(a) The signal at an m/z = 654.9802 corresponds to [**1**]$^+$. (b) Calculated isotopic distribution for [**1**]$^+$ (upper) and the amplifying experimental diagram for [**1**]$^+$ (bottom).

(a)

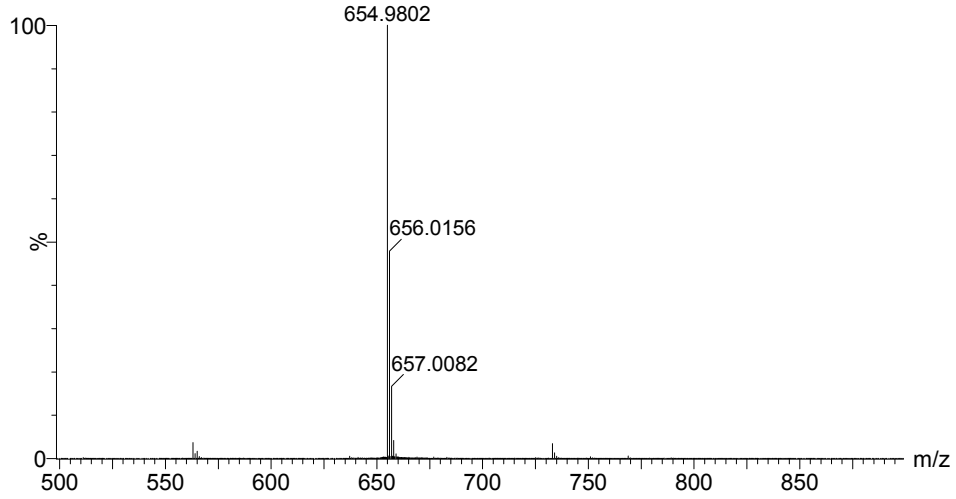

(b)

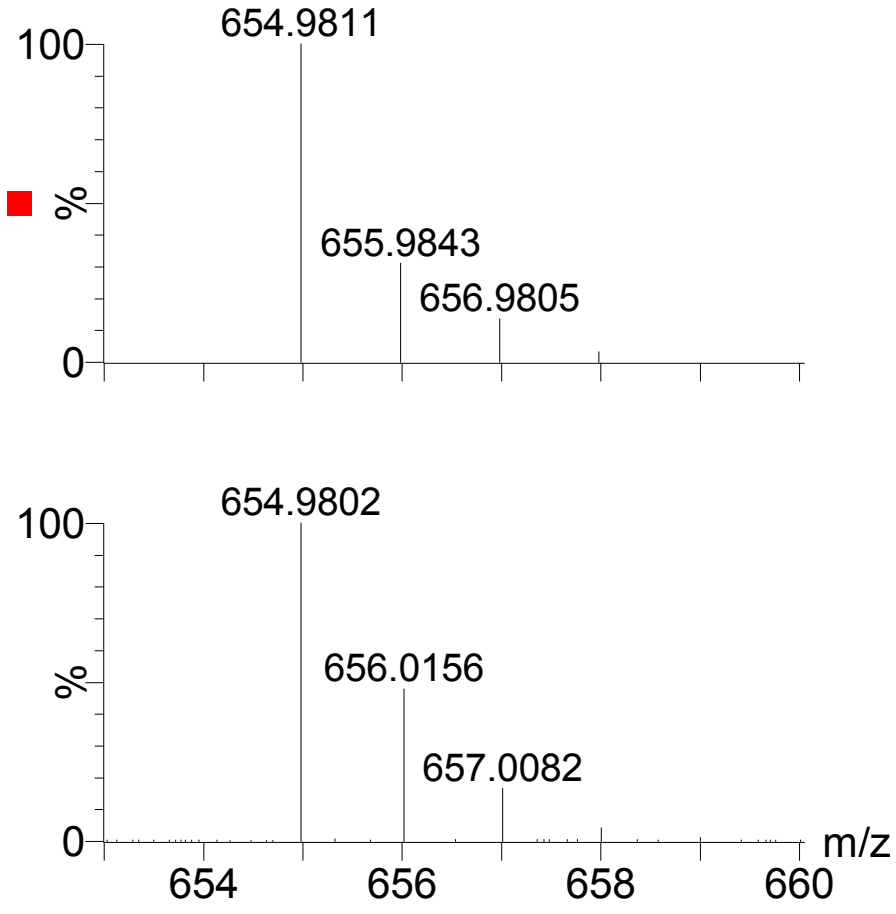

Fig. S7 ESI-HRMS of **3[PF_6]** in CH_2Cl_2

(a) The signal at an m/z = 511.0603 corresponds to [**3**]$^+$. (b) Calculated isotopic distribution for [**3**]$^+$ (upper) and the amplifying experimental diagram for [**3**]$^+$ (bottom).

(a)

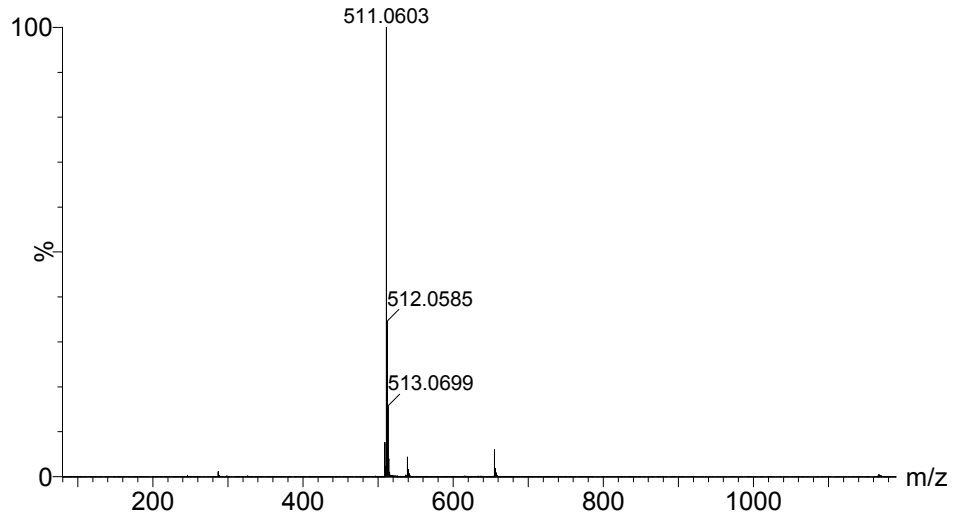

(b)

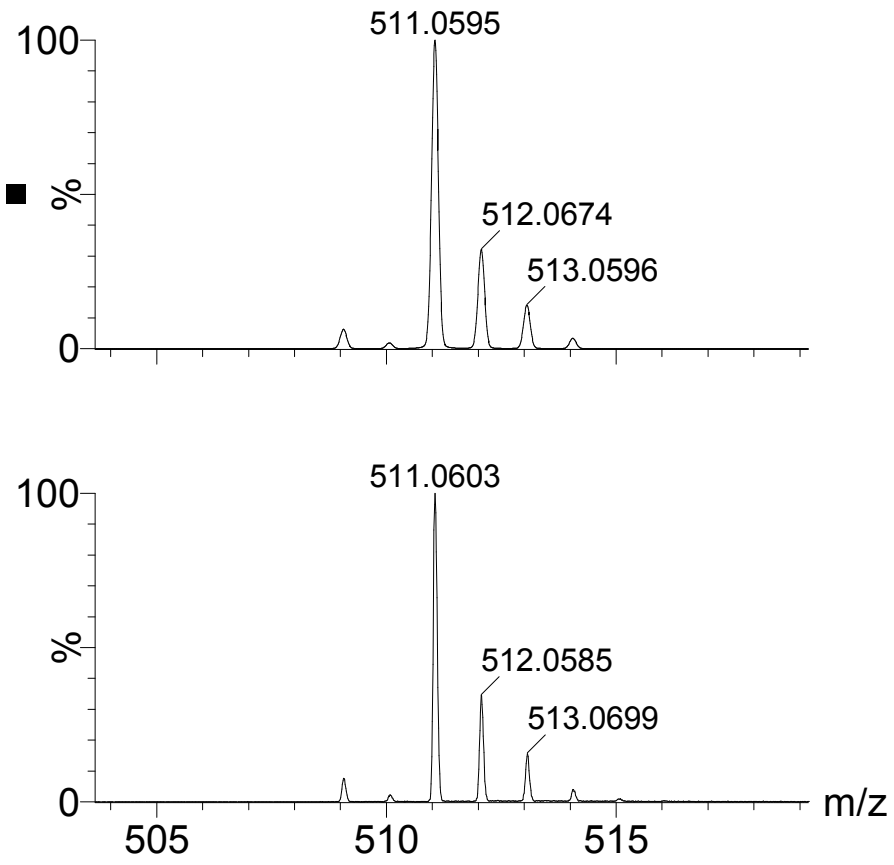

Fig. S8 ESI-HRMS of **4[BF_4]** in CH_2Cl_2

(a) The signal at an m/z = 529.0856 corresponds to [**4**]$^+$. (b) Calculated isotopic distribution for [**4**]$^+$ (upper) and the amplifying experimental diagram for [**4**]$^+$ (bottom).

(a)

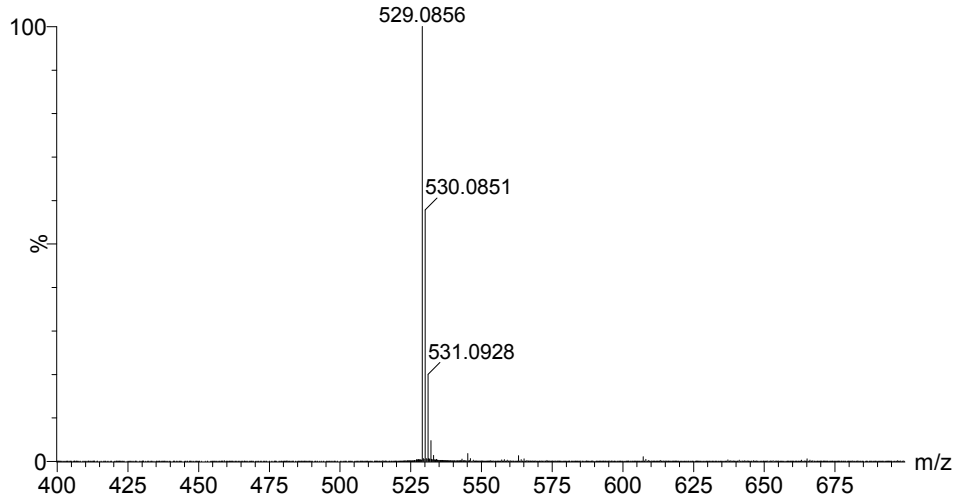

(b)

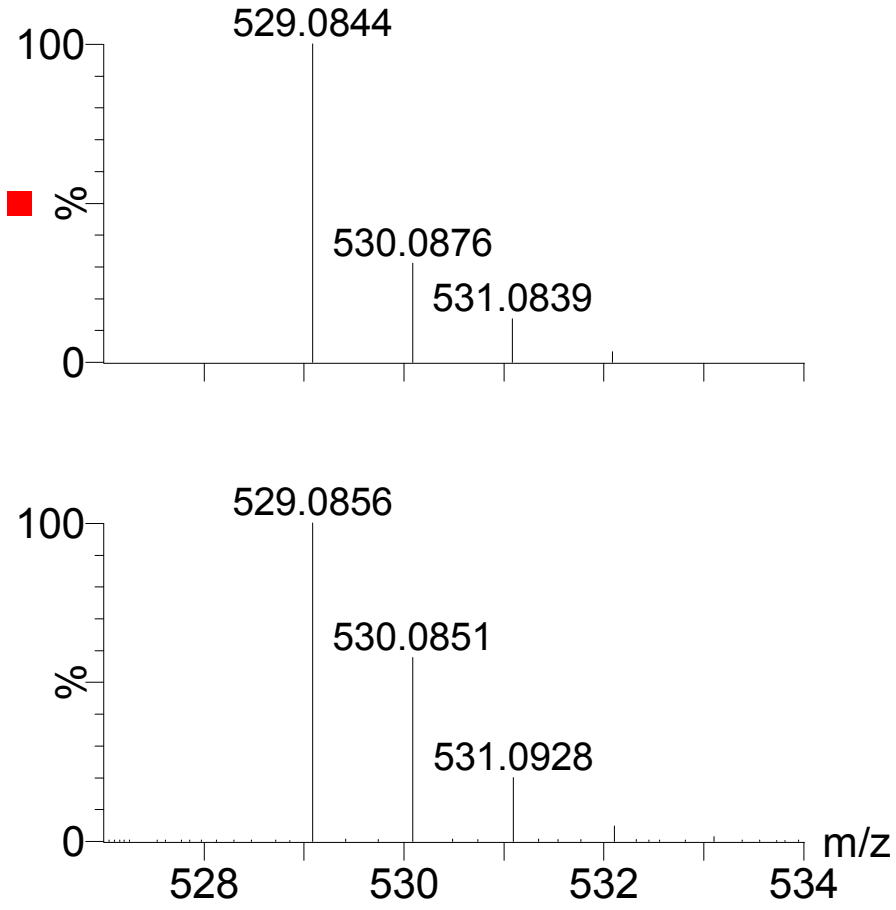

Fig. S9 The ^{1}H NMR spectrum of **1[PF_6]** in CD_2Cl_2

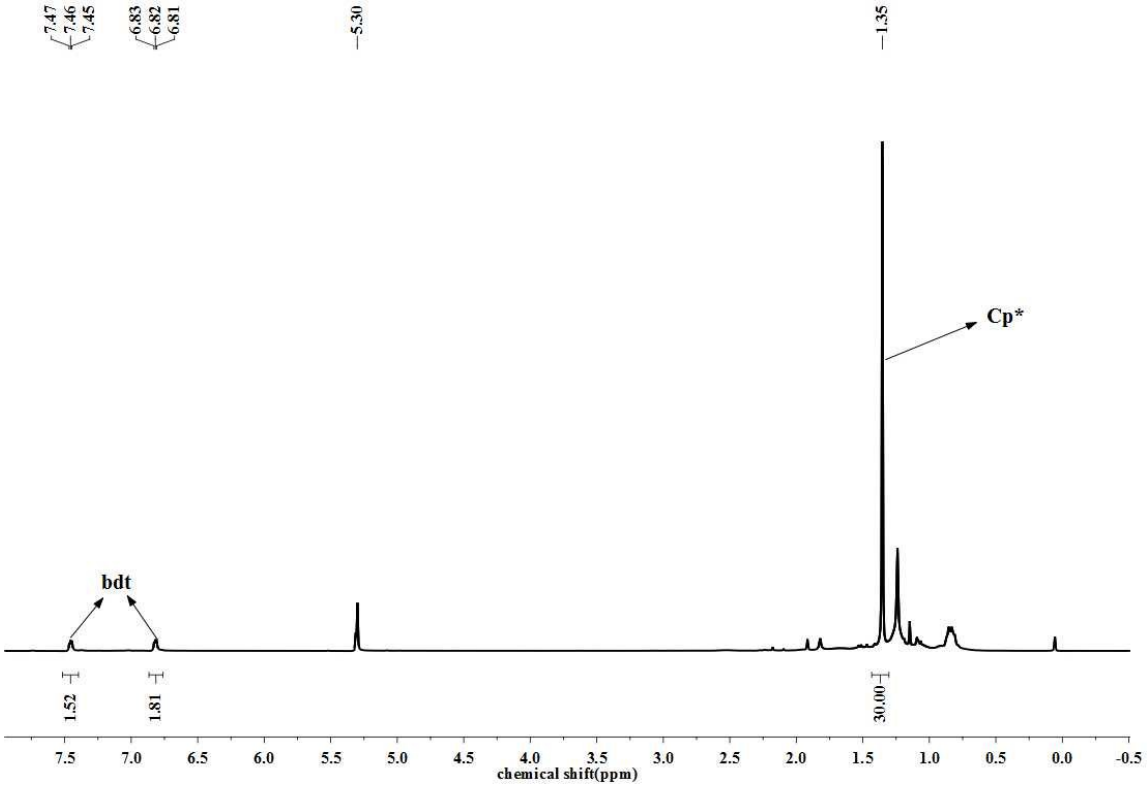

Fig. S10 The ^{1}H NMR spectrum of **2** in CD_2Cl_2

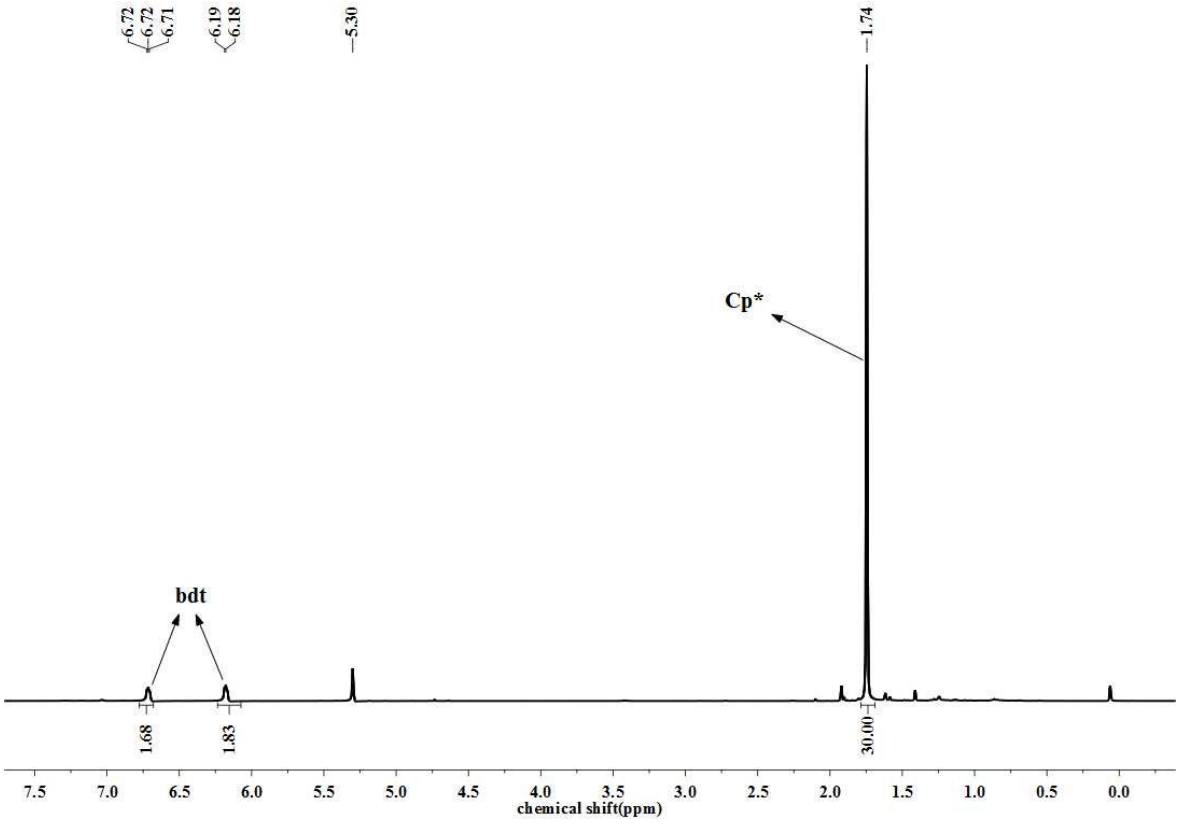

Fig. S11 The ^{1}H NMR spectrum of **3[PF_6]** in CD_2Cl_2

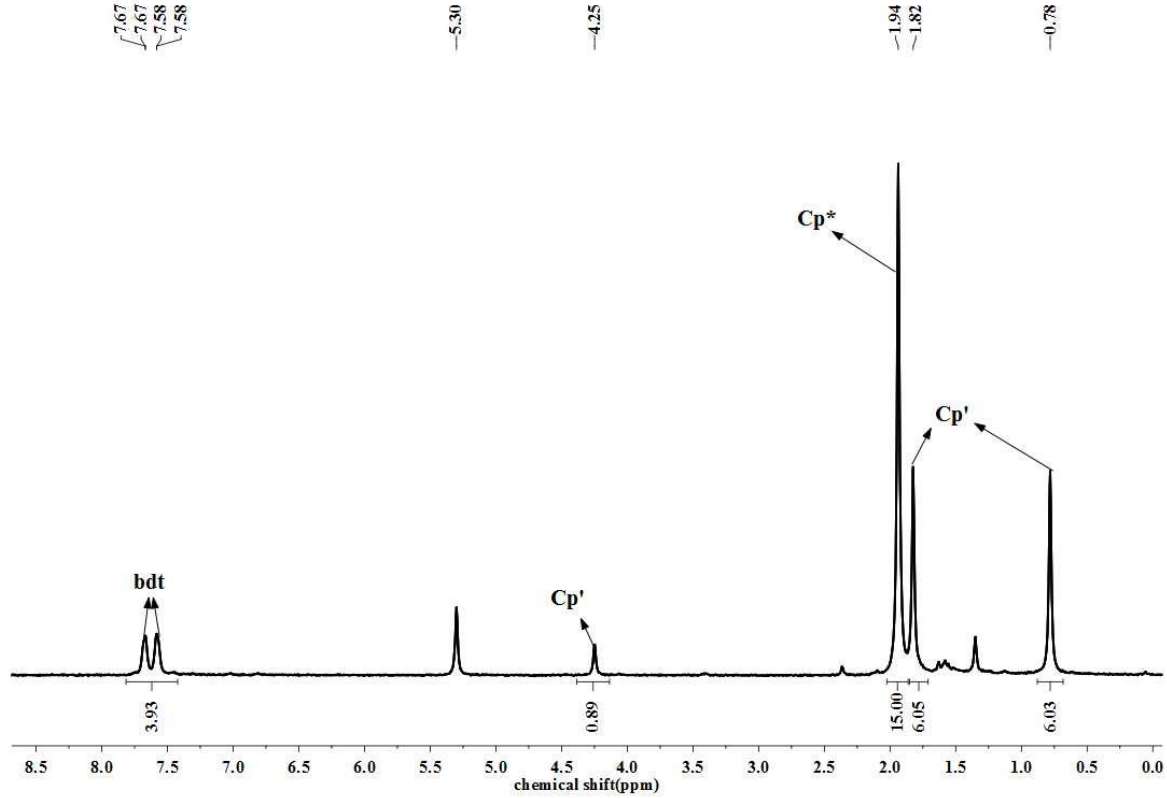

Fig. S12 The ^{1}H NMR spectrum of **4[BF_4]** in CD_2Cl_2

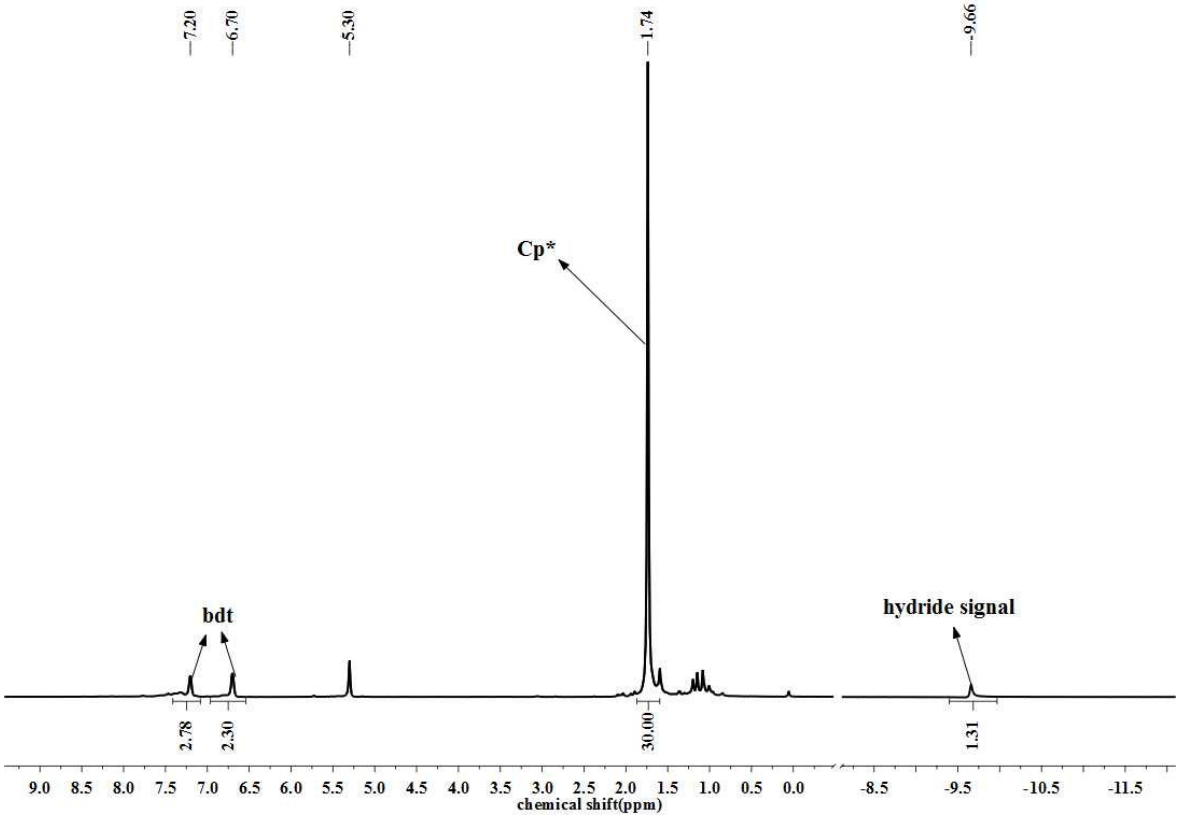

Fig. S13 The IR (film) spectrum of **2**

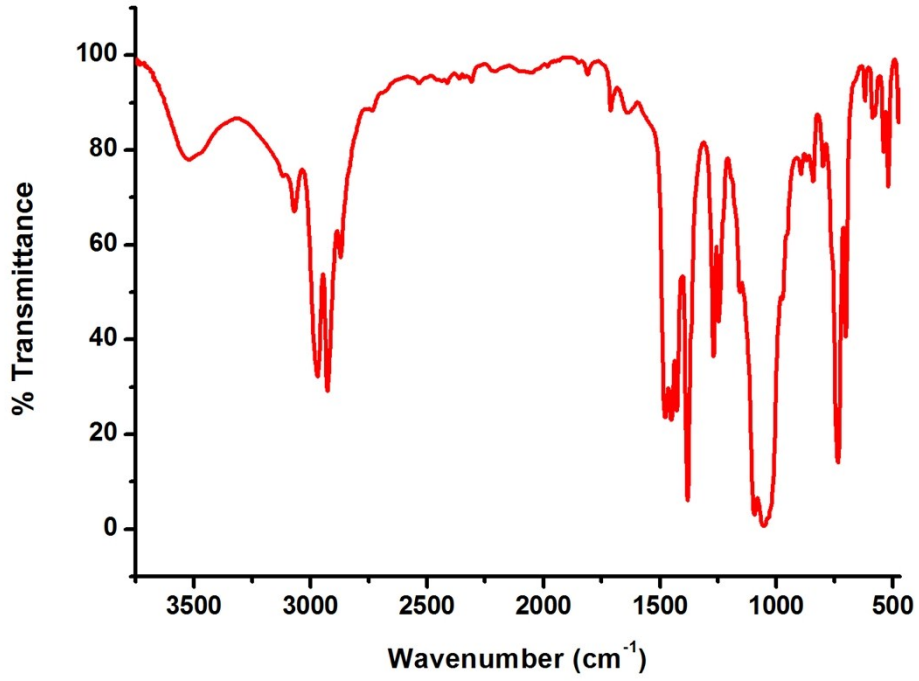

Fig. S14 The IR (film) spectrum of **3[PF_6]**

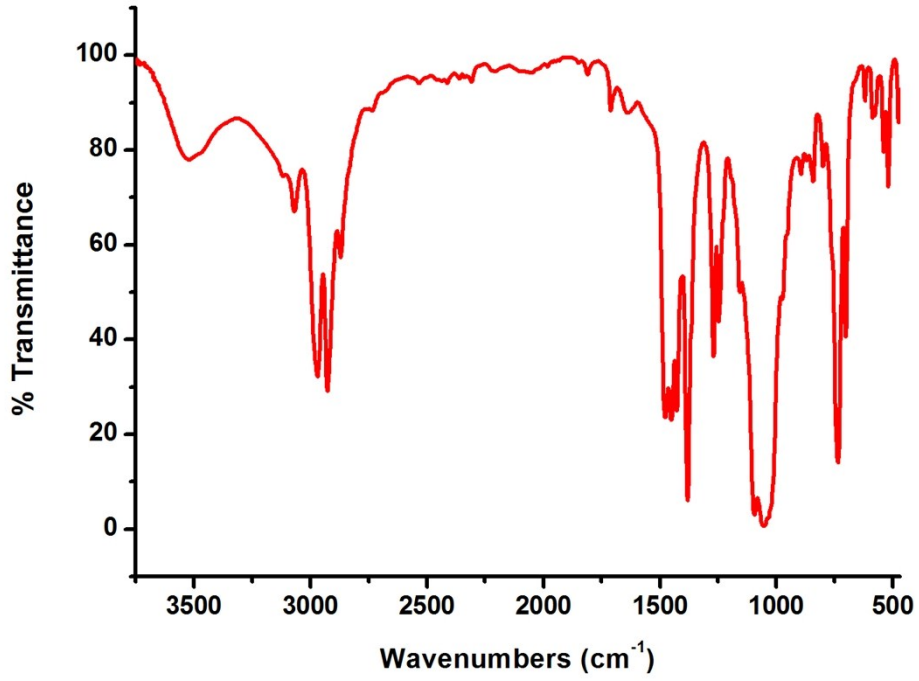

Fig. S15 The IR (film) spectrum of **4[BF_4]**

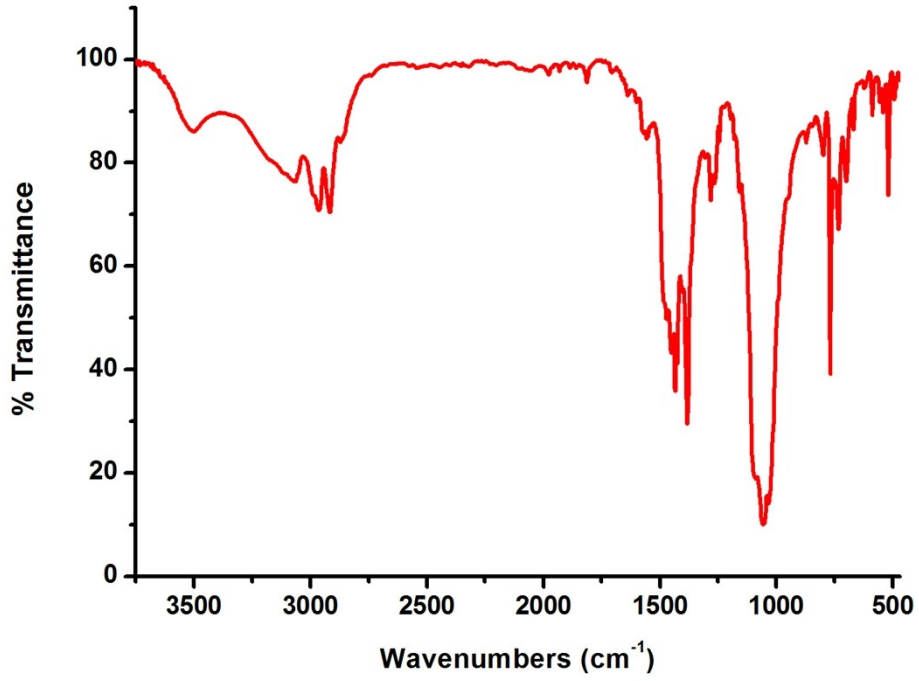

Fig. S16 The cyclic voltammogram of **1[PF_6]** (1 mM) in 0.1 M $^{n}Bu_4NPF_6/CH_2Cl_2$ at 25 °C with a scan rate of 100 mV s^{-1}

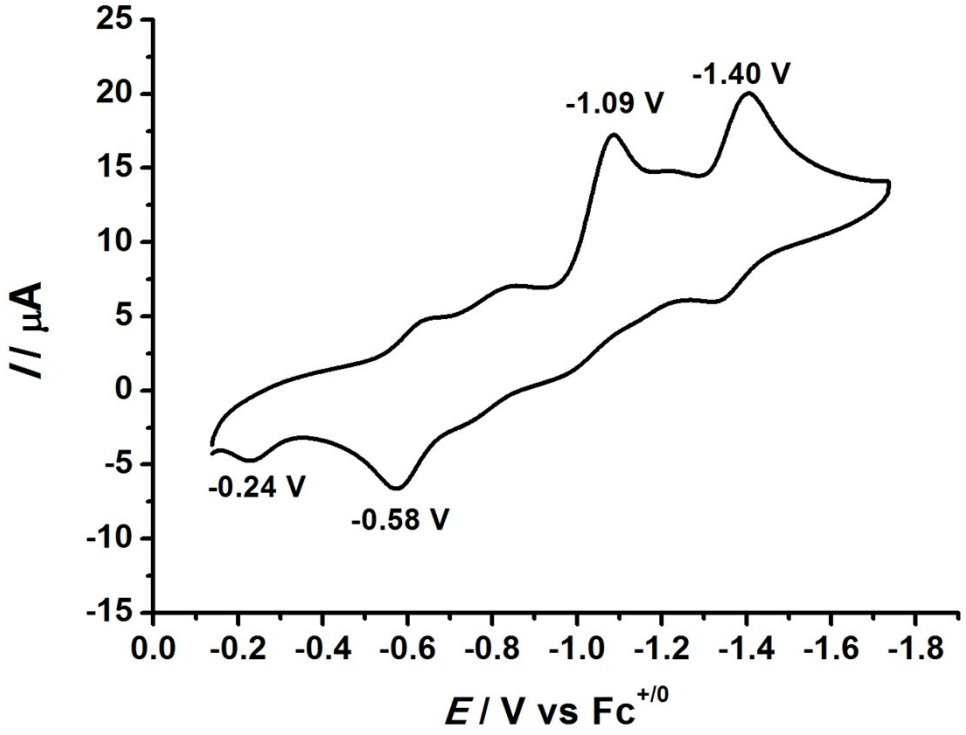

Fig. S17 The cyclic voltammogram of **3[PF_6]** (1 mM) in 0.1 M $^{n}Bu_4NPF_6/CH_2Cl_2$ at 25 °C with a scan rate of 100 mV s^{-1}

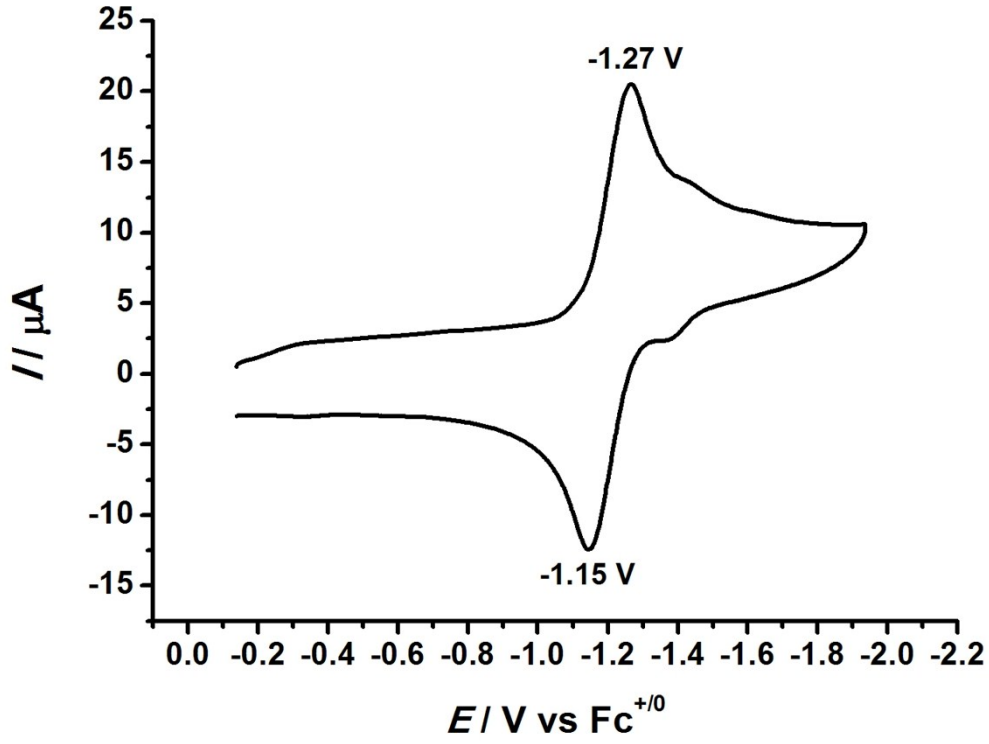

Fig. S18 The cyclic voltammogram of **4[BF_4]** (1 mM) in 0.1 M $^{n}Bu_4NPF_6/CH_2Cl_2$ at 25 °C with a scan rate of 100 mV s^{-1}

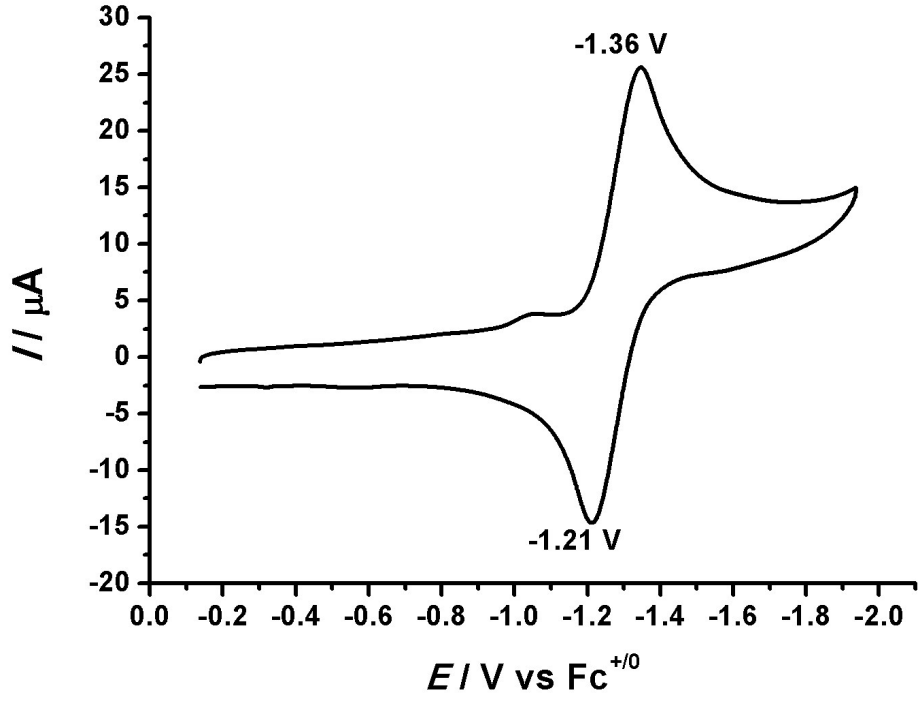

Fig. S19 The cyclic voltammogram of **4[BF_4]** (1 mM) in the presence of 1 equivalent of TFA in 0.1 M $^{n}Bu_4NPF_6/CH_2Cl_2$ at 25 °C with a scan rate of 100 mV s^{-1}

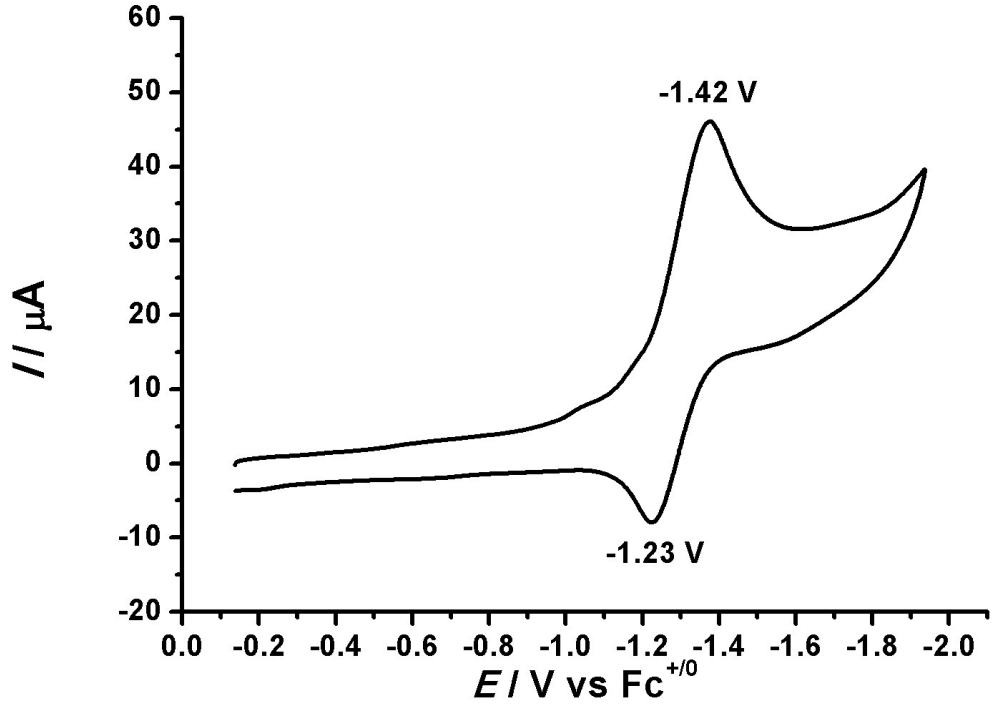

Fig. S20 The cyclic voltammogram of **4[BF_4]** (1 mM) in the presence of 3 equivalent of TFA in 0.1 M $^{n}Bu_4NPF_6/CH_2Cl_2$ at 25 °C with a scan rate of 100 mV s^{-1} (solid line: the recorded voltammogram; dash line: the first derivative of the forward scan)

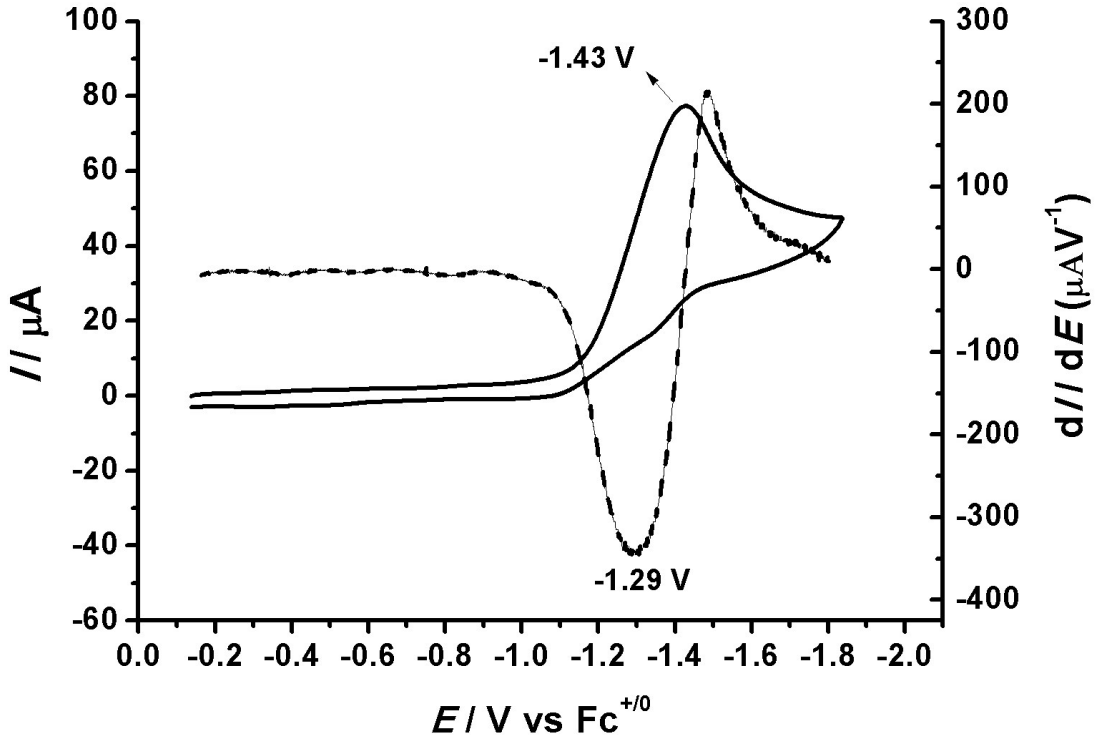

Fig. S21 The cyclic voltammogram of **4[BF_4]** (1 mM) in the presence of 1 equivalent of HBF_4 in 0.1 M $^n Bu_4NPF_6/CH_2Cl_2$ at 25 °C with a scan rate of 100 mV s^{-1}

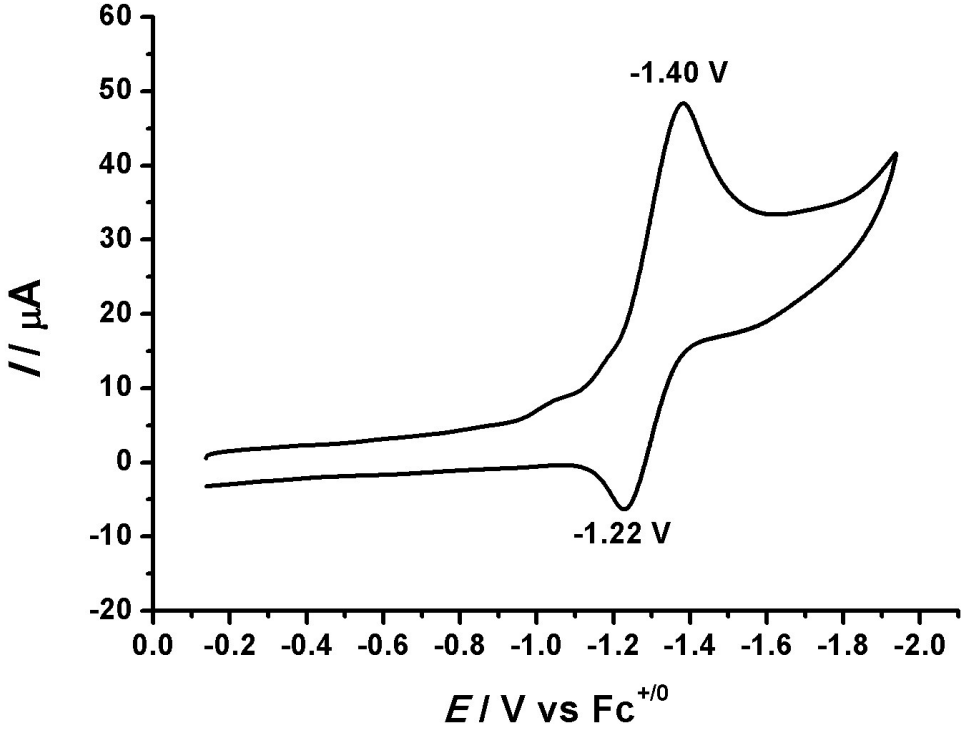

Fig. S22 Cyclic voltammograms of **4[BF_4]** (1 mM in 0.1 M $^n Bu_4NPF_6$ in CH_2Cl_2 under Ar, scan rate = 100 mv s^{-1}) with increments of HBF_4 (0, 1, 5, 10, 15, and 20 mM)

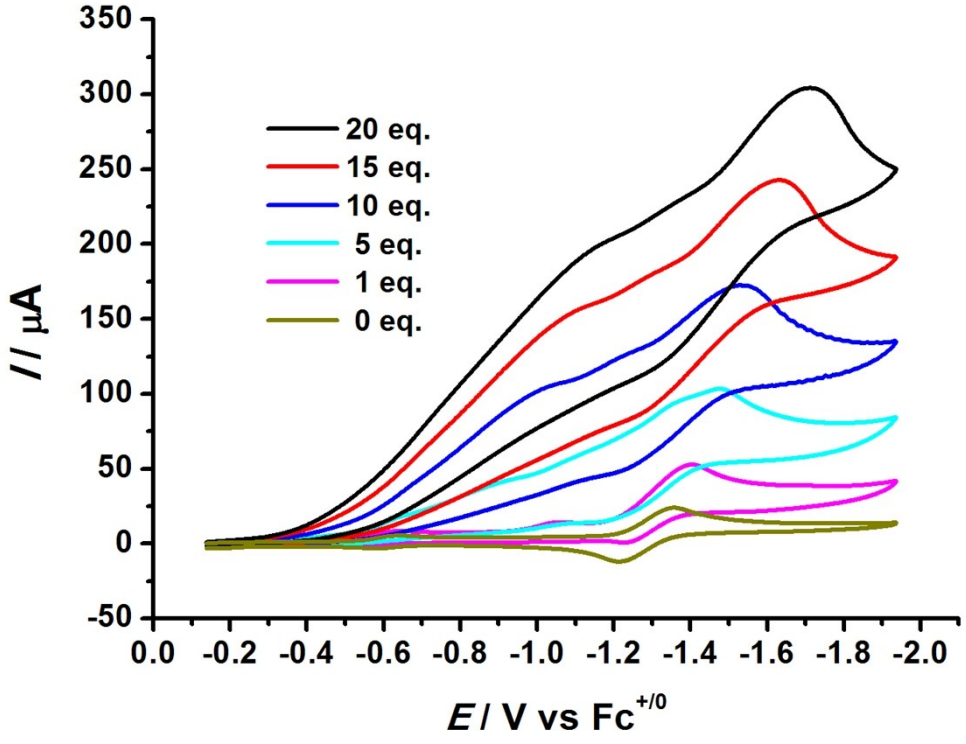

Fig. S23 The cyclic voltammogram of 30 mM TFA in 0.1 M $^{n}Bu_4NPF_6/CH_2Cl_2$ at 25 °C with a scan rate of 100 mV s^{-1}

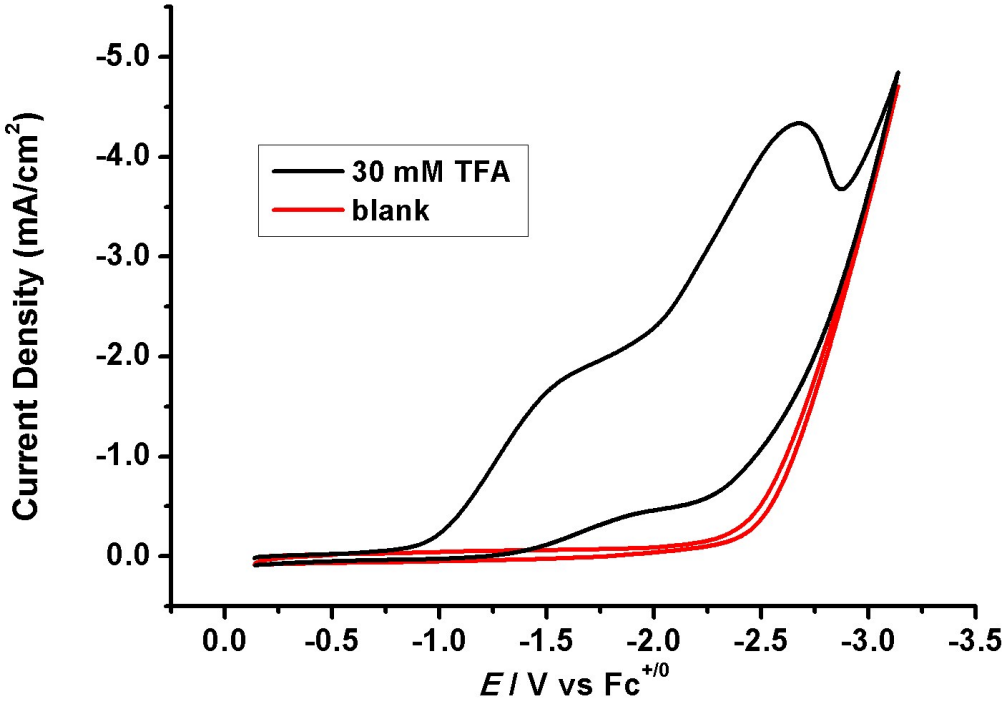

Fig. S24 The cyclic voltammogram of 25 mM HBF_4 in 0.1 M $^{n}Bu_4NPF_6/CH_2Cl_2$ at 25 °C with a scan rate of 100 mV s^{-1}

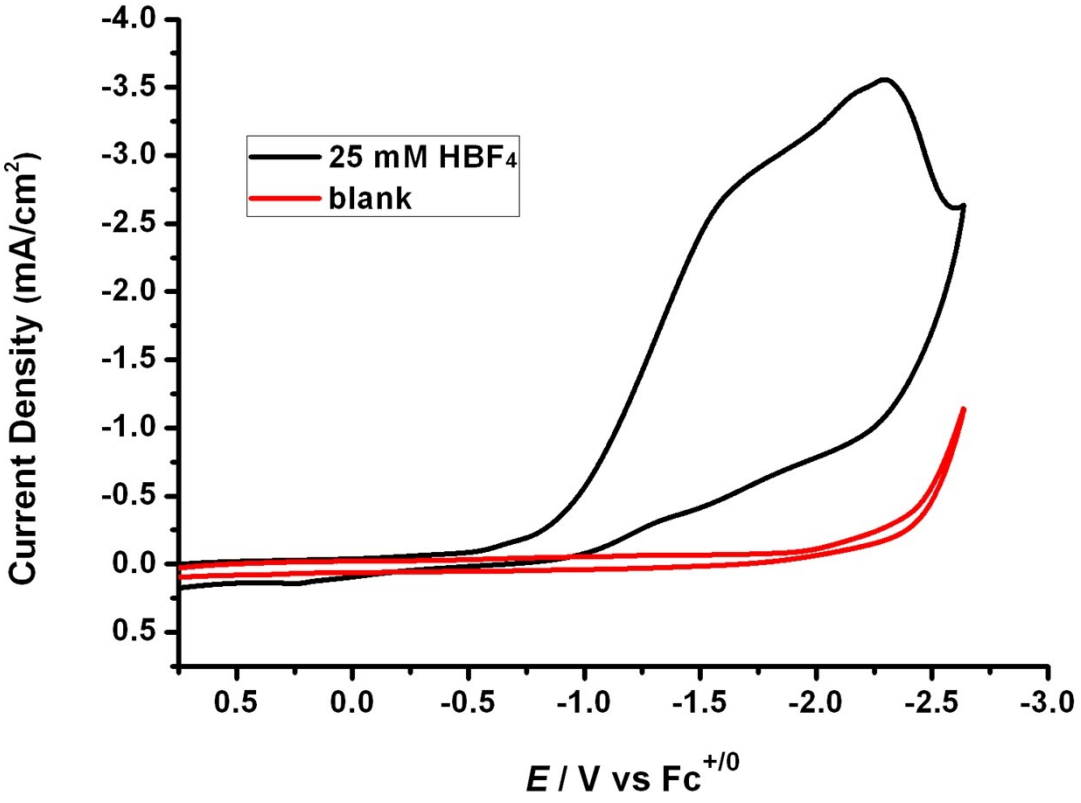

Fig. S25 The i-t curve for bulk electrolysis of TFA (30 mM) in the presence of **4[BF_4]** (1 mM) at –1.60 V

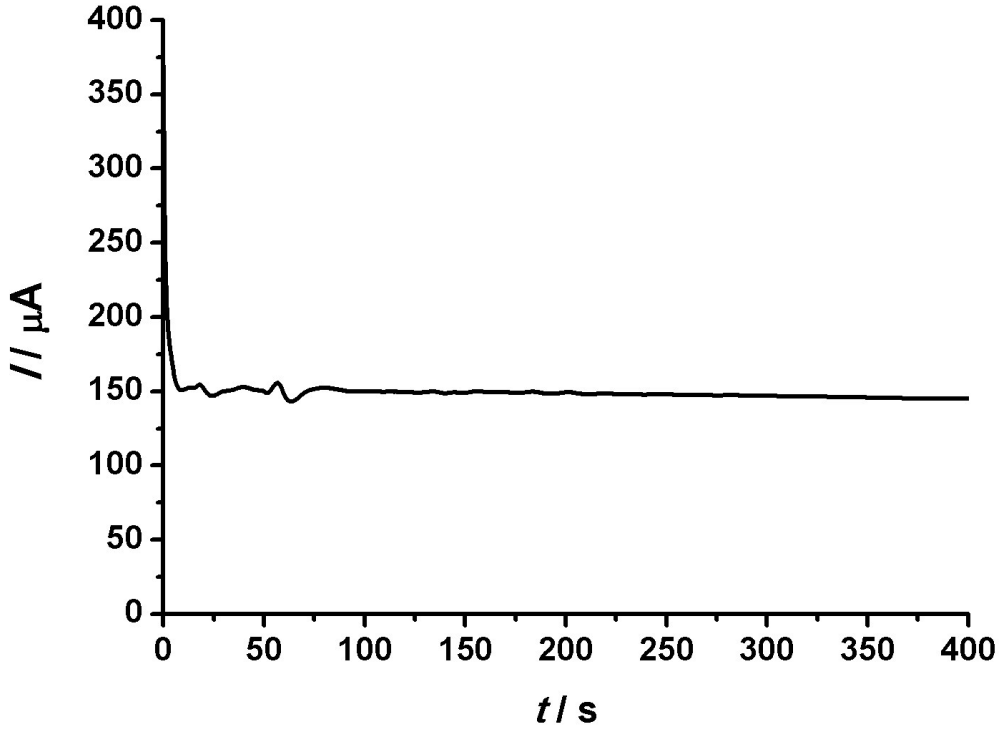

Fig. S26 GC data for the three-electrode cell after electrolysis, the first peak at 0.704 min was ascribed to hydrogen

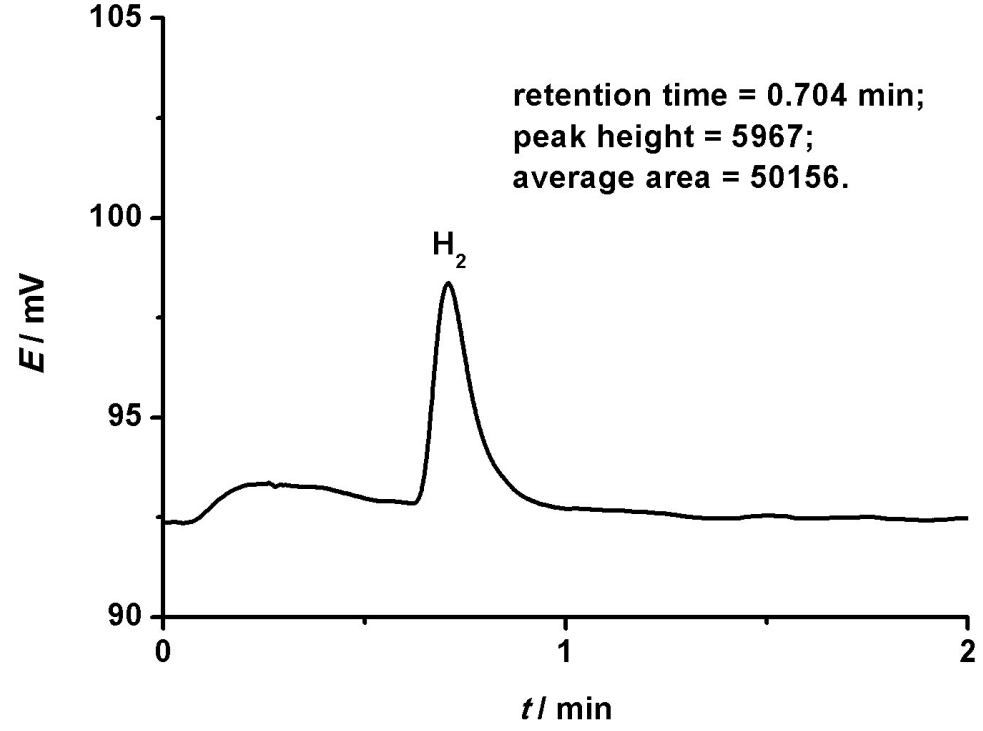

Fig. S27 The dependence of the catalytic peak currents for 30 mM TFA on the concentration of **4[BF_4]** in 0.1 M $^{n}Bu_4NPF_6/CH_2Cl_2$ at 25 °C with a scan rate of 100 mV s^{-1}

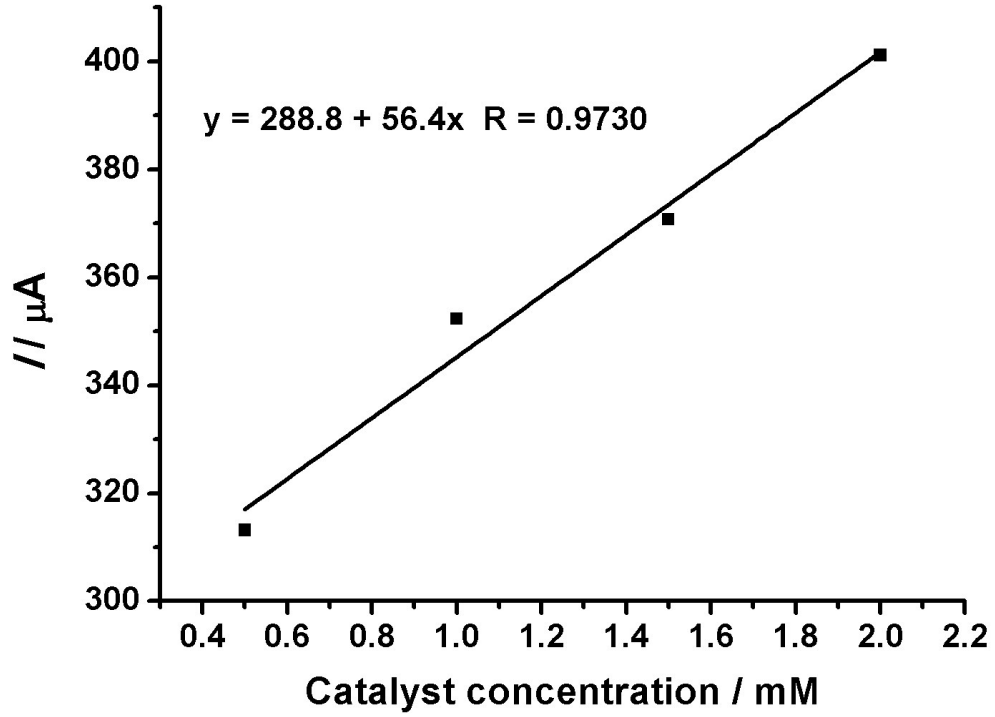

Fig. S28 The dependence of the catalytic peak currents for 1 mM **4[BF_4]** on the concentration of TFA in 0.1 M $^{n}Bu_4NPF_6/CH_2Cl_2$ at 25 °C with a scan rate of 100 mV s^{-1}

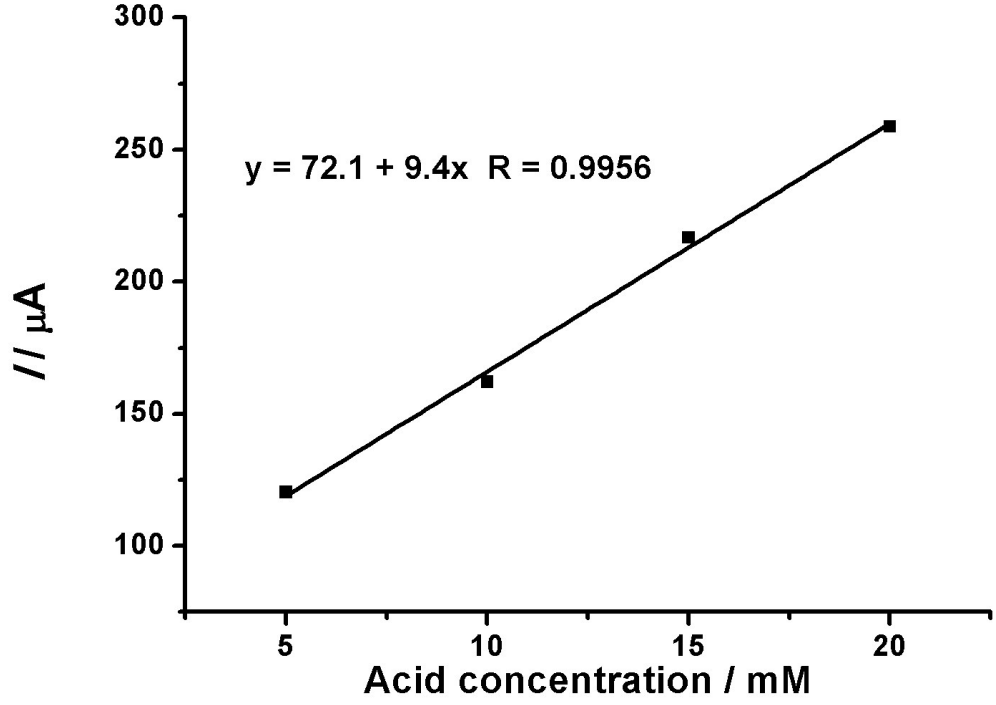

Fig. S29 Plot of the slopes from graph on left vs. $v^{-1/2}$. Rate constant for proton reduction by **4[BF_4]** is calculated from the slope of the equation for the linear fit

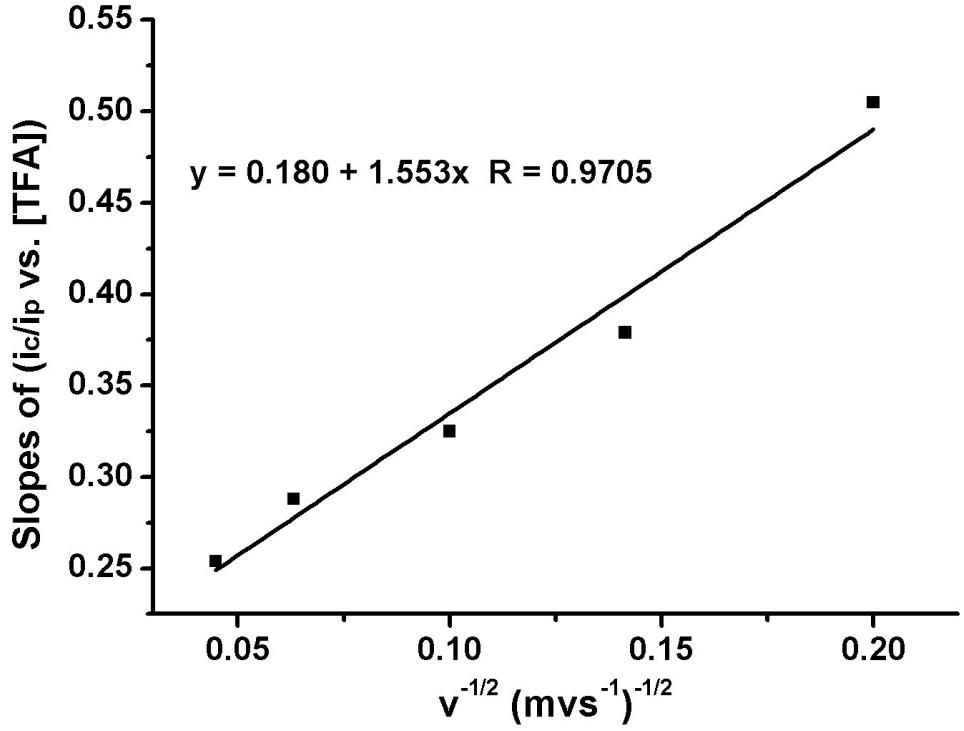

Fig. S30 The cyclic voltammogram of **3[PF_6]** (1 mM) in the presence of 1 equivalent of TFA in 0.1 M ^{n}Bu_4NPF_6/CH_2Cl_2 at 25 °C with a scan rate of 100 mV s^{-1}

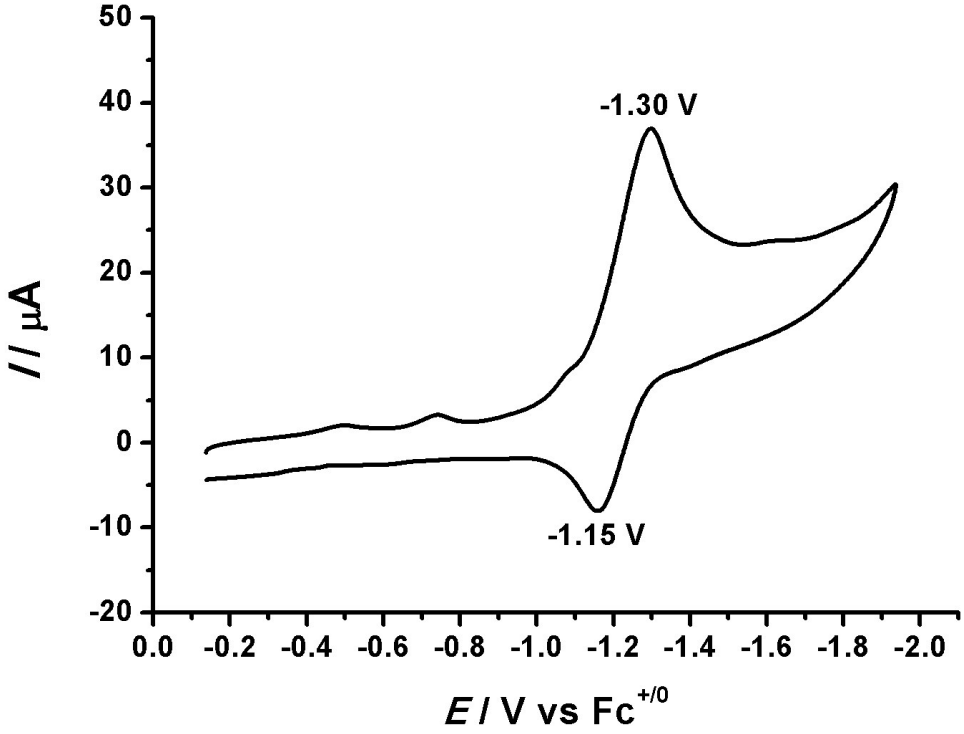

Fig. S31 Cyclic voltammograms of **3[PF_6]** (1 mM in 0.1 M $^nBu_4NPF_6$ in CH_2Cl_2 under Ar, scan rate = 100 mv s^{-1}) with increments of TFA (0, 1, 5, 10, 15, and 20 mM)

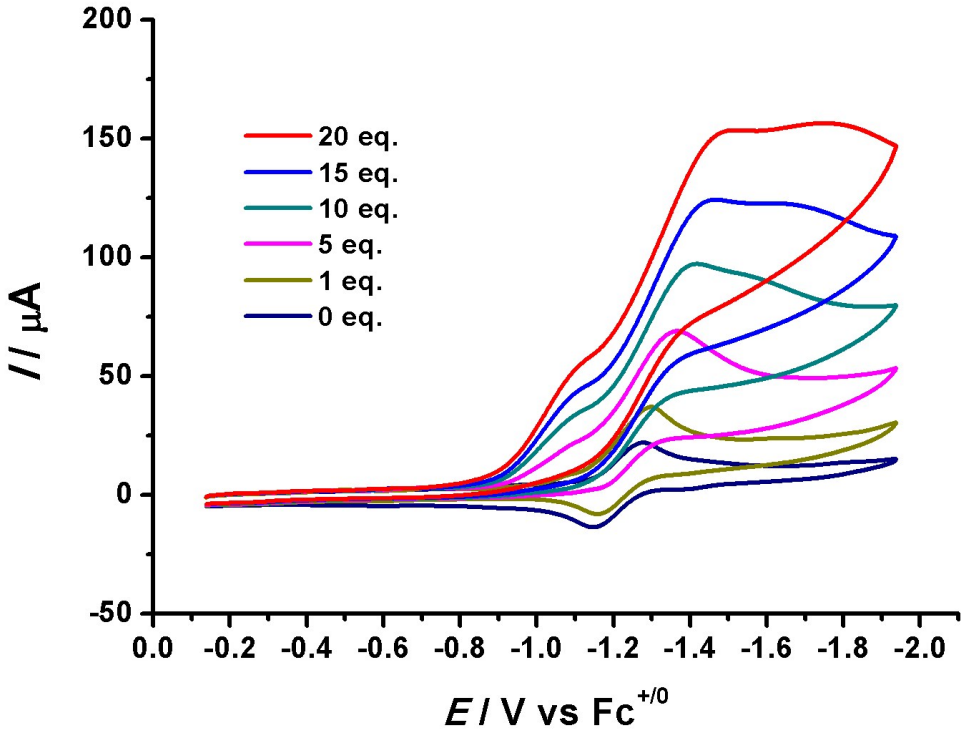

Fig. S32 The cyclic voltammogram of **3[PF_6]** (1 mM) in the presence of 1 equivalent of HBF_4 in 0.1 M $^nBu_4NPF_6/CH_2Cl_2$ at 25 °C with a scan rate of 100 mV s^{-1}

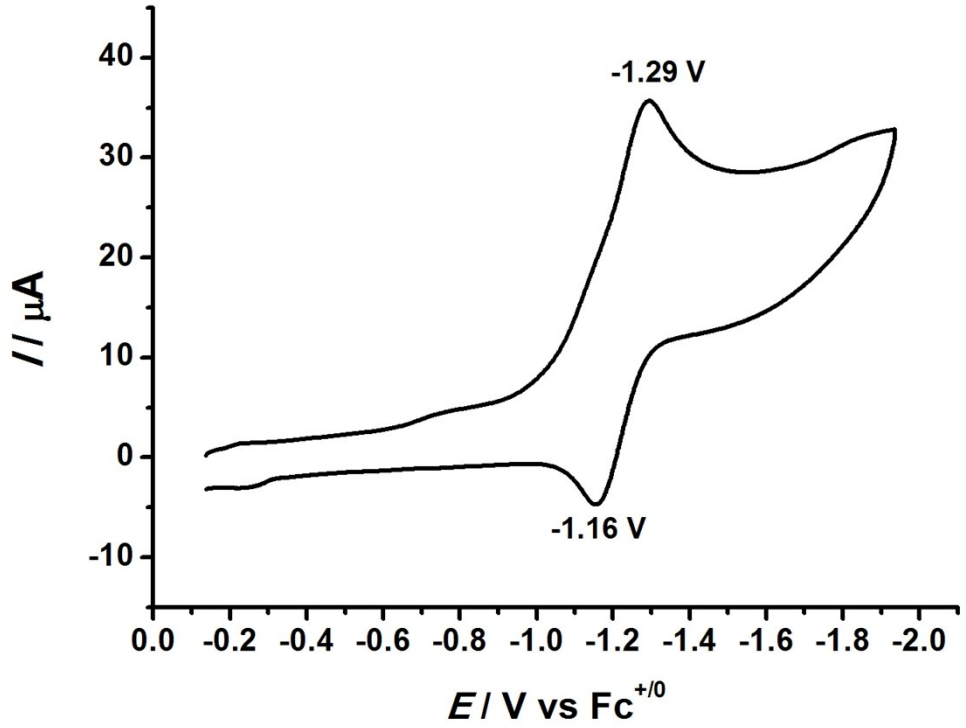

Fig. S33 Cyclic voltammograms of **3[PF_6]** (1 mM in 0.1 M $^nBu_4NPF_6$ in CH_2Cl_2 under Ar, scan rate = 100 mv s^{-1}) with increments of HBF_4 (0, 1, 5, 10, 15, 20, 25, and 30 mM)

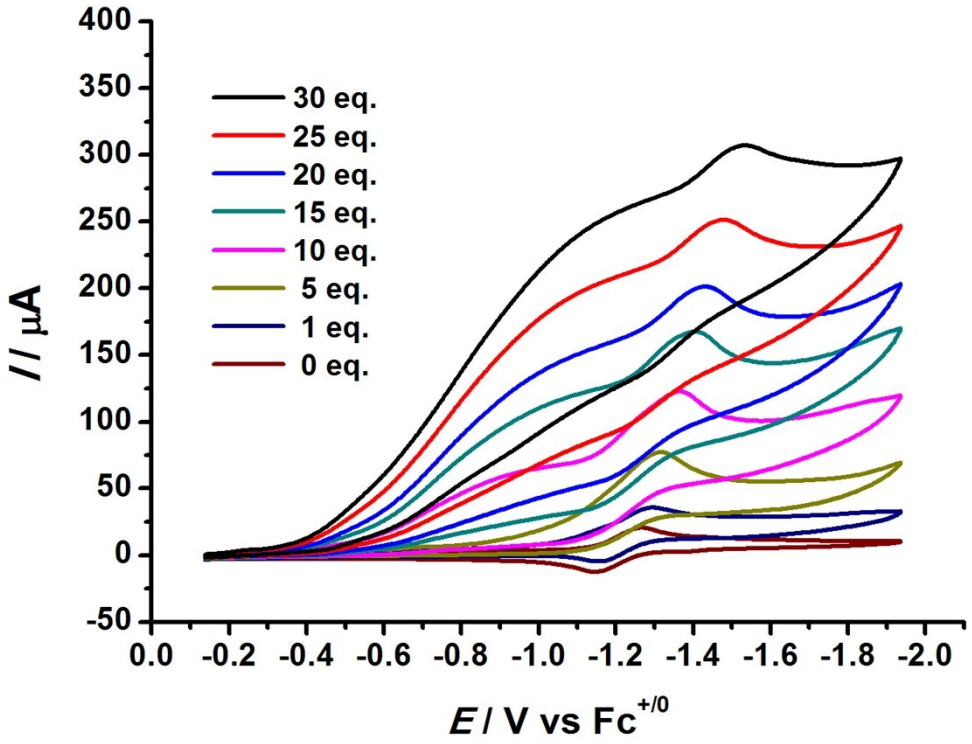

Fig. S34 The dependence of the catalytic peak currents for 1 mM **3[PF_6]** and **4[BF_4]** on the concentration of acid (HBF_4 and TFA) in CH_2Cl_2

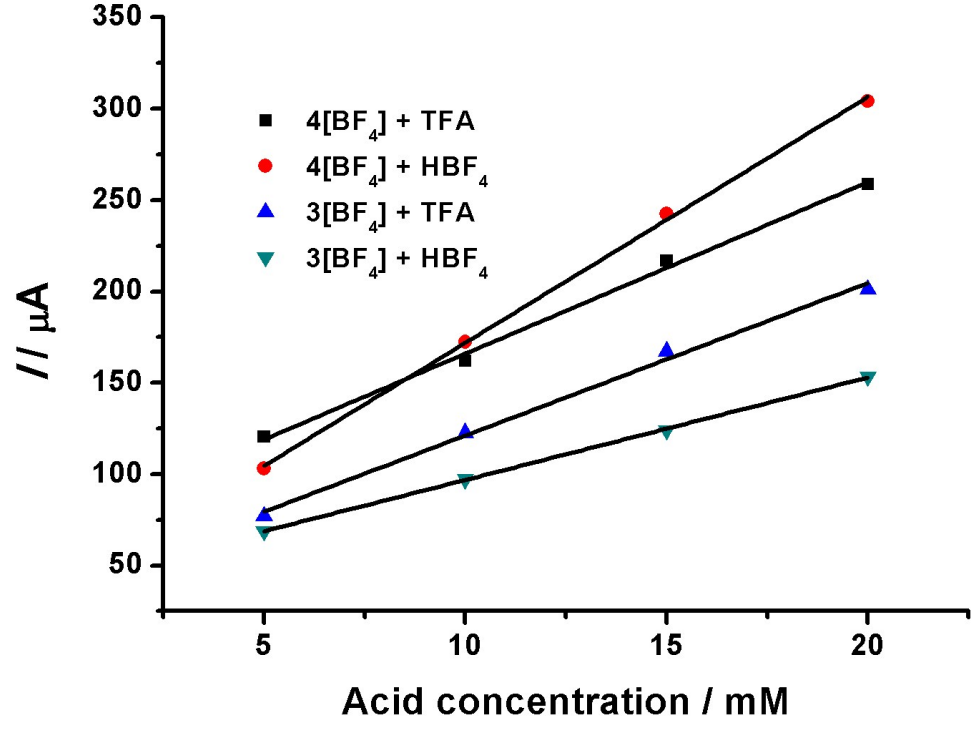

Fig. S35 Cyclic voltammograms of **4[BF_4]** (1 mM in 0.1 M $^{n}Bu_4NPF_6$ in CH_2Cl_2 under Ar, scan rate = 100 mv s^{-1}) with increments of TFA (a: c_{TFA} = 10 mM, black line: before a short bulk electrolysis, blue line: after a short bulk electrolysis; b: c_{TFA} = 30 mM, black line: before a short bulk electrolysis, red line: after a short bulk electrolysis.)